Journal of Colloid and Interface Science 426 (2014) 181–189

Contents lists available at ScienceDirect

Journal of Colloid and Interface Science

www.elsevier.com/locate/jcis

The distinct effects of Mn substitution on the reactivity of magnetite in heterogeneous Fenton reaction and Pb(II) adsorption

Xiaoliang Liang [a], Zisen He [a,c], Gaoling Wei [b], Peng Liu [a,c], Yuanhong Zhong [a,c], Wei Tan [a,c], Peixin Du [a,c], Jianxi Zhu [a], Hongping He [a,*], Jing Zhang [d]

[a] Key Laboratory of Mineralogy and Metallogeny, Guangzhou Institute of Geochemistry, Chinese Academy of Sciences, Guangzhou 510640, China
[b] Guangdong Institute of Eco-Environmental and Soil Sciences, Guangzhou 510650, China
[c] University of Chinese Academy of Sciences, Beijing 100049, China
[d] Institute of High Energy Physics, Chinese Academy of Sciences, Beijing 100049, China

ARTICLE INFO

Article history:
Received 20 December 2013
Accepted 26 March 2014
Available online 2 April 2014

Keywords:
Manganese substituted magnetite
Heterogeneous Fenton reaction
Adsorption
Heavy metal
EXAFS

ABSTRACT

In this study, a series of Mn substituted magnetites were synthesized and used in catalyzing the heterogeneous Fenton degradation of acid orange II and Pb(II) adsorption, in order to investigate the effect of Mn substitution on the reactivity of magnetite. The valence and local environment of both Fe and Mn in the spinel structure of magnetite were investigated by X-ray absorption fine structure (XAFS) spectroscopy. The incorporation of Mn did not change the valence and local structure of Fe in the synthetic magnetite, while Mn was in the valences of +2 and +3. The Mn distribution on the octahedral sites of magnetite surface increased with the increase in Mn content. The Mn introduction led to an improvement of catalytic activity of magnetite. The sample with the minimum Mn content displayed the best efficiency in ·OH production and the degradation of acid orange II, while the other substituted samples did not show obvious difference in their catalytic performance. The adsorption capacity of magnetite samples toward Pb(II) gradually increased with the increase in Mn content. The above influences of Mn substitution on the reactivity of magnetite were discussed in views of the variations in microstructural environment and physicochemical properties.

1. Introduction

The spread of a wide range of contaminants (e.g., organic pollutants and heavy metals) in surface water and groundwater has become a critical issue worldwide, due to the fast population growth and rapid development of industrialization [1]. Thus, it is imperative to develop novel, efficient and friendly materials and technologies to remove these contaminants. A number of iron oxides including goethite [2,3], hematite [4,5], magnetite [6,7], ferrihydrite [8,9] and lepidocrocite [10,11] were applied to adsorb heavy metal species and initiate the advanced oxidation processes (AOPs) as heterogeneous catalysts for organic degradation.

Compared to other iron oxides, magnetite has several interesting structural features. Magnetite contains both Fe^{2+} and Fe^{3+} in spinel structure, with Fe^{2+} occupying the octahedral site and Fe^{3+} distributed between octahedral and tetrahedral sites. Fe^{2+} plays an important role as an electron donor to initiate the AOPs [12]. The accommodation of Fe^{2+} and Fe^{3+} on the octahedral sites allows the Fe species to be reversibly oxidized and reduced while keeping the structure unchanged [13]. In most natural magnetites, iron cations are isomorphously substituted by divalent (Co, Ni, Mn, etc.), trivalent (V, Cr, etc.) and tetravalent (Ti) cations [14]. These substitutions may vary the microstructure and physicochemical properties of magnetite and accordingly affect its surface reactivity in heavy metal adsorption and catalyzing AOPs. As a common constituent in soils and sediments, magnetite plays a vital role in the adsorption and redox behavior of heavy metals and organic contaminants [15].

Heterogeneous Fenton reaction, a typical advanced oxidation technology, is novel and promising for the destruction of organic contaminants in wastewaters [16]. In Fenton reaction, H_2O_2 is activated to generate radicals, especially ·OH, according to the classic Haber–Weiss mechanism [17]. ·OH has a quite high oxidation potential (2.8 eV) and can completely oxidize the organic pollutants in aqueous medium. Magnetite is especially efficient

* Corresponding author. Present Address: Key Laboratory of Mineralogy and Metallogeny, Guangzhou Institute of Geochemistry, Chinese Academy of Sciences, Guangzhou 510640, China. Fax: +86 20 85290708.
E-mail addresses: liangxl@gig.ac.cn (X. Liang), hezisen881026@163.com (Z. He), gaoling_wei@126.com (G. Wei), liupeng@gig.ac.cn (P. Liu), zhongyuanhong@gig.ac.cn (Y. Zhong), tanwei@gig.ac.cn (W. Tan), dupeixin@gig.ac.cn (P. Du), zhujx@gig.ac.cn (J. Zhu), hehp@gig.ac.cn (H. He), jzhang@ihep.ac.cn (J. Zhang).

http://dx.doi.org/10.1016/j.jcis.2014.03.065
0021-9797/

in catalyzing the heterogeneous Fenton reaction, ascribed to the presence of highly active Fe^{2+} species on magnetite surface and the fast electron transfer between Fe^{2+} and Fe^{3+} on the octahedral sites [13,18]. The incorporation of transition metals in magnetite obviously affects the Fenton reactivity of magnetite. The introduction of Co [13], Ti [19,20], V [18] and Cr [21] improves the Fenton catalytic activity of magnetite, while Ni shows an inhibitory effect [13]. Such distinct effects greatly depend on the oxidation states and occupancy of substituting cations [22,23]. Therefore, the experimental determination of cation distribution in the spinel structure and their oxidation states is an interesting challenge. But the conventional methods, e.g., electron spin resonance (ESR), X-ray photoelectron spectroscopy (XPS) and Mössbauer spectroscopy are restricted to certain elements or not possible to perform under *in situ* condition [24]. X-ray absorption fine structure (XAFS) spectrum is a powerful tool for the characterization of chemical environment and is composed of X-ray absorption near edge structure (XANES) and extended X-ray absorption fine structure (EXAFS) spectroscopes. XANES provides the information about overall oxidation states and site symmetry of the absorbing central atom. EXAFS reflects the crystal structure and local environment of the absorbing central atom [25]. The combination of XANES and EXAFS can present detailed description of atomic structure in substituted magnetite. From our previous publications [18,20,26], among the common substituting metals, the valence and distribution of Mn in magnetite structure are the most complicated. In this study, XAFS characterization was carried out to investigate the oxidation states and coordination environment of metal cations in Mn substituted magnetite ($Fe_{3-x}Mn_xO_4$). Moreover, through the batch experiments of acid orange II (AOII) decolorization and ·OH generation in heterogeneous Fenton system catalyzed by $Fe_{3-x}Mn_xO_4$, the relationship between local atomic structure of $Fe_{3-x}Mn_xO_4$ and its heterogeneous Fenton activity was discussed.

Besides being used as Fenton catalyst, magnetite is an important attenuator of heavy metals. Magnetite has been applied in the adsorption of various heavy metals, e.g., Cr(VI) [27], Hg(II) [28], As(V) [25], Sb(V) [29], Se(IV) [30] and U(VI) [31]. The adsorption mechanism includes surface site binding [32], electrostatic interaction [33], modified ligand combination [34] and oxidation–reduction interaction [35,36]. Some substitutions have made obvious variations on the physicochemical properties of magnetite surface [26,37]. For instance, some substituting cations (e.g., Cr^{3+} and Ti^{4+}) increase the surface hydroxyl amount of magnetite. The surface hydroxyl groups are functional groups of iron oxides, due to its vital role of surface acidity in heavy metal adsorption. The specific surface area of magnetite is also varied by some substitutions, ascribed to the decrease in magnetism and thus particle aggregation. Such changes probably affect the adsorption properties of magnetite for heavy metals. But to the best of our knowledge, few studies have grasped this issue. In this study, Mn substituted magnetites were tested for the removal of Pb(II) in aqueous solution. Through the characterization of surface physicochemical properties, the effect of Mn substitution on the adsorption capacity of magnetite for Pb(II) was illustrated. The obtained results in this study will be of great significance for well understanding the interaction mechanism of magnetite-group minerals in the environmental self-purification process and their application in pollution protection.

2. Materials and methods

2.1. Sample preparation

All the chemicals and reagents were of analytical grade. For the synthesis of Fe_3O_4, 0.90 mol L^{-1} of $FeSO_4{\cdot}7H_2O$ was dissolved in an HCl solution. 1.0 mL of hydrazine was added to prevent Fe^{2+} oxidation, and the pH was set below 1.0 to prevent Fe^{2+} oxidation, and hydroxide precipitation. This solution was heated to 90–100 °C. Equal volume of a solution containing 4.0 mol L^{-1} NaOH and 0.90 mol L^{-1} $NaNO_3$ was added dropwise (10 mL min^{-1}) into the heated iron solution and the reaction was maintained at 90 °C for 5 h, while stirring at a rate of 500 rpm. Then the solution was cooled down to room temperature. During the reaction, a N_2 flux was passed through to prevent Fe^{2+} oxidation. The particles were then separated by centrifugation at 3500 rpm for 5 min and washed with boiling distilled water, followed by an additional centrifugation. After 3–4 washings, the particles were collected and dried in a vacuum oven at 100 °C for 24 h [26,38]. The obtained sample was labeled as FM0. The preparation of Mn substituted magnetites also followed the above procedure, except dissolving predetermined amount of $MnSO_4{\cdot}7H_2O$ in HCl solution with $FeSO_4{\cdot}7H_2O$. The total metal concentration of Fe and Mn in HCl solution should be kept at 0.90 mol L^{-1}. The obtained samples with different substitution extents were labeled as FM1, FM2, FM3 and FM4 and their detailed descriptions are shown in Table 1. All the samples were ground and passed through a 200 mesh screen.

2.2. Characterization methods

The chemical composition of synthetic samples was analyzed on Varian Vista ICP-AES (Inductively Coupled Plasma Atomic Emission Spectroscopy). XRD patterns were recorded on a Bruker D8 advance diffractometer using Cu Kα radiation scanning from 10° to 80° at a step of 1°min^{-1}. Specific surface area was analyzed by using the BET method using N_2 adsorption/desorption at 77 K on an ASAP 2020 instrument. The surface hydroxyl amount was analyzed by thermogravimetric and differential scanning calorimetry (TG–DSC) on a Netzsch STA 409 PC instrument.

The point of zero charge (PZC) of magnetite samples was detected by the potentiometric acid/base titration method [39]. The sample was mixed with NaCl solutions of different concentrations (c) to obtain 1 g°L^{-1} magnetite suspensions in which the final concentrations of $NaClO_4$ were 0.001, 0.010, and 0.100 mol L^{-1}. When the change in pH value did not exceed 0.02 pH unit in 5 min, the amount of acid (HCl 0.1 mol L^{-1}) or base (NaOH, 0.1 mol L^{-1}) added and the potential value of the suspension were recorded and used to calculate the adsorption amounts of H^+ and OH^-.

Table 1
Chemical composition and main physicochemical properties for Mn substituted magnetite samples.

Samples	C_{Mn} (wt%)	C_{Fe} (wt%)	Lattice parameter a_0 (nm)	Crystal size (nm)	Specific surface area ($m^2\ g^{-1}$)	Surface hydroxyl amount (%)	pH_{pzc}
FM0	0.0	72.3	8.411	43	16.6	0.64	6.9
FM1	6.0	63.9	8.414	40	15.0	1.42	7.0
FM2	11.7	56.3	8.423	37	18.3	2.16	7.0
FM3	17.9	51.9	8.425	35	22.0	2.27	7.1
FM4	20.0	51.5	8.429	33	26.0	2.31	7.1

XAFS spectra of synthetic samples and reference compounds were measured on the beamline 1W1B of Beijing Synchrotron Radiation Facility (BSRF). The spectra were acquired at room temperature in transmission mode, where an ion-chamber detector filled with 100% N_2 was used. For the Fe (7112 eV) K-edge, a 100% Ar filled Lytle ion-chamber detector with Mn X-ray filters and soller slits were used. The chromator energy was calibrated using a Fe foil. For the Mn K-edge (6539 eV), a Mn metal foil reference was used to calibrate the monochromator. The obtained XAFS data was analyzed with IFEFFIT software package.

2.3. Heterogeneous Fenton reaction

The degradation of AOII ($C_{16}H_{11}N_2NaO_4S$) was performed in a conical flask at 25 °C. The dye solution was stirred for 1 h in the presence of magnetite particles to achieve adsorption equilibrium. Then H_2O_2 was added into the solution to initiate the degradation. The magnetite dosage was 1.0 g L^{-1} and the concentrations of AOII and H_2O_2 were 0.2 and 75 mmol L^{-1}, respectively. The initial pH (7.0) of solution was adjusted by H_2SO_4 and NaOH. At given intervals, the reaction solution was sampled for AOII concentration analysis by UV–Vis spectroscopy (PE Lambda 850) at a wavelength of 484 nm. The concentrations of leaching Fe and Mn cations were determined on a PE-3100 Flame Atomic Absorption Spectrophotometer (FAAS) with the hollow-cathode lamps operate at the wavelength of 248.3 and 279.5 nm. The ·OH concentration was analyzed by High Performance Liquid Chromatography (HPLC) [40,41]. The experiment details of operation are provided in Text A.1 in Supplementary Data.

2.4. Pb(II) adsorption

Stock solution of Pb(II) (1.0 g L^{-1}) was prepared by dissolving lead nitrate ($Pb(NO_3)_2$) in deionized water. The adsorption experiment of Pb(II) was conducted with initial Pb(II) concentration of 10–500 mg/L^{-1} and adsorbent concentration of 1 g L^{-1} at 25 °C and pH 4.5 with magnetic stirring at 600 rpm. The suspension (50 mL) was constantly stirred for 1 h, predetermined time for achieving adsorption equilibrium. Then the solution samples were withdrawn and passed through a 0.22 μm PTFE filter. The residual aqueous Pb(II) concentration was determined on PE-3100 FAAS with the hollow-cathode lamps operate at the wavelength of 223.1 nm. All the adsorption and degradation experiments were performed in triplicate.

3. Results and discussion

3.1. Sample characterization

The chemical compositions for all the prepared magnetite samples are displayed in Table 1. The increase in Mn content is followed by a simultaneous decrease in Fe content, suggesting that Mn cations have replaced Fe cations.

The XRD characteristic of all the magnetite samples (Fig. 1) mostly corresponds to the standard card of magnetite (JCPDS: 19-0629), indicating that these samples mainly have spinel structure. But for samples with high Mn content (FM3 and FM4), a new phase of feitknechtite with the reflections 2θ around 19° and 34° (JCPDS: 18-0804) appears. The reflection peaks of new phase become stronger with the increase in Mn content, suggesting that besides magnetite, some Mn cations exist as feitknechtite $Mn(OH)_3$ in the samples with a high Mn content. But from the XRD pattern characteristics, the content of magnetite in FM3 and FM4 is obviously in the majority.

Table 1 also shows the lattice parameter a_0, crystal size, BET specific surface area and pH_{PZC} for all the samples. With the increase in Mn content, the lattice parameter a_0 and specific surface area increase while the crystal size decreases.

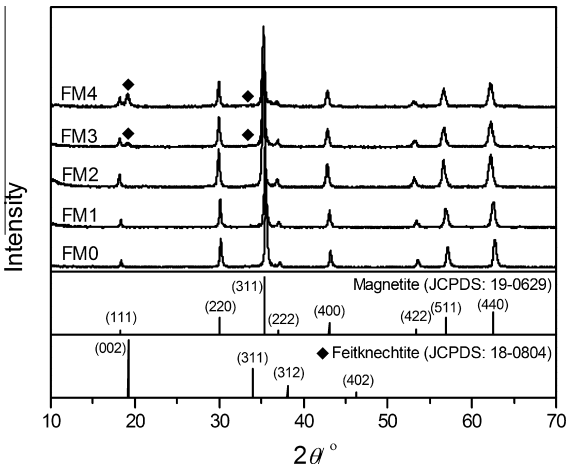

Fig. 1. XRD patterns for Mn substituted magnetite samples.

3.2. XAFS spectroscopy

In the normalized Fe K-edge XANES spectra of all the magnetite samples (Fig. 2A), the pre-edge peak around 7110 eV is attributed to the quadrupole transition from 1*s* to 3*d* orbital [42,43]. The absorption K-edge at 7122 eV does not show any obvious energy shift, indicating that the substitution of Mn cations does not affect the valences of iron cations.

The Fe K-edge EXAFS spectra and their Fourier-transform (FT) curves are shown in Fig. 2B and C. On the FT curves, the first peak in the range of 1.0–1.5 Å presents the information on the Fe—O bonds. The peaks near 1.1 and 1.5 Å arise dominantly from 4-coordinated and 6-coordinated Fe—O subshells. The second peak is a doublet, providing information on the Fe—Fe shell [25]. The first component of the doublet near 3.1 Å corresponds to the Fe_{oct}—Fe_{oct} subshell, while the second component at 3.6 Å is ascribed to several contributions, dominantly to the Fe_{tet}—Fe_{oct} and Fe_{tet}—Fe_{tet} subshells.

In order to obtain quantitative information, the fitting of Fe K-edge EXAFS spectra was performed (Fig. 2B and C), and the fitted parameters are given in Table 2. The fitted values of two different Fe—O distances are 1.90 ± 0.02 and 2.05 ± 0.02 Å, which are consistent with the theoretical values of Fe—O bond length at the tetrahedral and octahedral sites of magnetite [25]. Four Fe—Fe subshells fit well with the experimental results, with a Fe—Fe coordination number of about 3.5–4.2 at bond distance of 2.99 ± 0.01 Å, 7.2–8.7 at 3.49 ± 0.02 Å, 7.0–8.0 at 5.19 ± 0.01 Å and 4.0–6.0 at 5.50 ± 0.02 Å (Table 2). The Fe—Fe bond distances are close to those of magnetite structure reported in literatures [25,44]. With the increase in Mn content, the XAFS spectra and fitting parameters show no distinct variations. This illustrates that the valence and atomic environment of iron in magnetite have not been distinctly changed by Mn substitution.

Fig. 3 shows the normalized XANES spectra for substituted magnetite samples and reference compounds. Among these samples, their profiles and location of Mn K-edge vary obviously. The energy position of XANES spectra depends on the binding energy of absorbing atom and hence on the oxidation state [45]. The Mn K-edge position of magnetite samples is located between those of MnO and Mn_2O_3 and gradually shifts with the increase in Mn content. This illustrates that the valences of Mn are +2 and +3, and the average valence increases with the increase in Mn content.

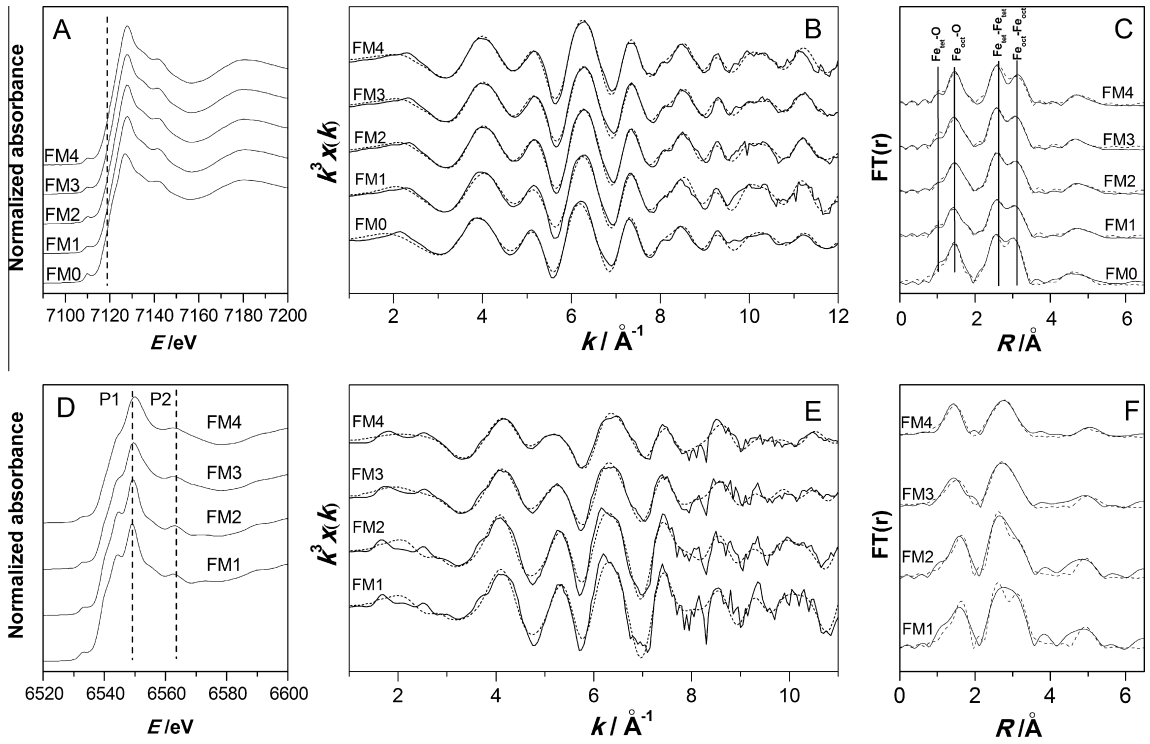

Fig. 2. Normalized Fe K-edge XANES spectra (A), EXAFS spectra (B) and Fourier-transform of EXAFS spectra (C), and normalized Mn K-edge XANES spectra (D), EXAFS spectra (E) and the Fourier-transform of EXAFS spectra (F) for Mn substituted magnetite samples (solid lines: experimental curves; dash lines: fitting curves).

Table 2
Fe K-edge EXAFS fitting results for Mn substituted magnetite samples.

Samples	FM0			FM1			FM2			FM3			FM4		
	N[a]	R[b] (Å)	σ^{2c} (Å^2)	N	R (Å)	σ^2 (Å^2)	N	R (Å)	σ^2 (Å^2)	N	R (Å)	σ^2 (Å^2)	N	R (Å)	σ^2 (Å^2)
Fe—O	1.4(5)	1.88(2)	0.003(1)	1.2(1)	1.89(2)	0.003(1)	1.3(1)	1.90(2)	0.003(1)	1.2(2)	1.90(2)	0.003(1)	1.3(2)	1.91(2)	0.003(2)
Fe—O	4.3(5)	2.03(2)	0.009(4)	3.6(3)	2.04(2)	0.006(2)	3.8(3)	2.05(2)	0.006(3)	3.7(4)	2.04(2)	0.006(3)	3.8(3)	2.05(2)	0.007(3)
Fe—Fe	3.7(7)	2.97(2)	0.010(4)	3.5(4)	2.99(2)	0.010(2)	3.7(3)	3.00(2)	0.011(3)	3.5(6)	2.99(2)	0.008(2)	4.2(5)	3.00(1)	0.011(3)
Fe—Fe	8.6(8)	3.46(2)	0.010(2)	8.2(6)	3.48(2)	0.009(2)	7.7(7)	3.49(2)	0.009(2)	8.7(9)	3.48(2)	0.009(2)	7.2(8)	3.51(2)	0.008(2)
Fe—Fe	12(1)	5.15(4)	0.011(3)	8(1)	5.18(3)	0.012(2)	8(1)	5.19(3)	0.012(2)	7(1)	5.18(4)	0.012(2)	8(1)	5.21(2)	0.012(2)
Fe—Fe	8(1)	5.46(4)	0.011(6)	5(1)	5.49(4)	0.014(5)	6(1)	5.51(3)	0.015(5)	4(1)	5.49(4)	0.020(5)	5(1)	5.52(3)	0.013(4)

N[a]: Coordination number.
R[b]: Bond length.
σ^{2c}: Debye–Waller factor.

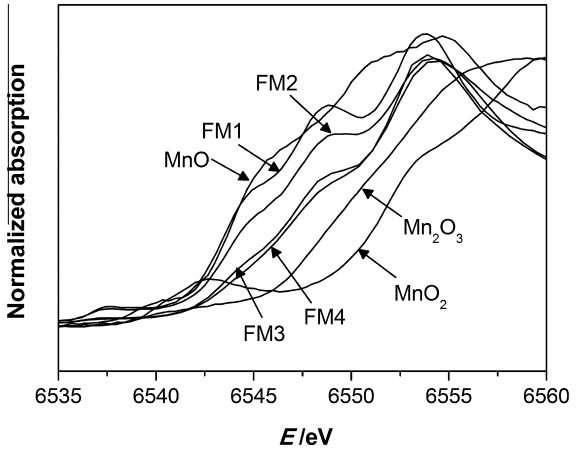

Fig. 3. Normalized Mn K-edge XANES spectra of Mn substituted magnetite samples and reference samples.

Through the linear combination fitting [46], the proportions of Mn^{2+} to Mn^{3+} in FM1, FM2, FM3 and FM4 are 85:15, 83:17, 60:40 and 52:48, respectively, suggesting an increase in Mn^{3+} proportion.

The K-edge profile of FM1 and FM2 with low Mn content is quite identical, but evidently different from those of FM3 and FM4 with high Mn content (Fig. 2D). Compared to FM1 and FM2, the maxima of peaks P1 and P2 are less pronounced in the XANES of FM3 and FM4. This is mainly ascribed to the decrease in coordination number of Mn—O and Mn—Mn/Fe shells [47].

The Mn K-edge EXAFS spectra and their FT curves (Fig. 2E and F) also reveal the difference between samples with low Mn content (FM1 and FM2) and those with high Mn content (FM3 and FM4). For FM3 and FM4, the oscillation intensity shows a significant decrease. The first peak on the FT curves is around 1.6 Å for FM1 and FM2, and 1.4 Å for FM3 and FM4, suggesting that the length of Mn—O bond is shortened with Mn content increase. The second peak is arisen dominantly from the Mn—Mn/Fe shells. With the increase in Mn content, the intensity of second peak around 3 Å decreases and a small peak at 2.2 Å appears. This is mainly ascribed to the increase in static disorder and decrease in coordination number of Mn—Mn/Fe shells [48].

Table 3
Mn K-edge EXAFS fitting results for Mn substituted magnetite samples.

Samples	FM1			FM2			FM3			FM4		
	N	R (Å)	σ^2 (Å^2)	N	R (Å)	σ^2 (Å^2)	N	R (Å)	σ^2 (Å^2)	N	R (Å)	σ^2 (Å^2)
Mn—O	5.3(6)	2.08(1)	0.008(4)	5.4(6)	2.08(1)	0.010(4)	4.6(6)	1.95(1)	0.011(3)	4.5(7)	1.94(1)	0.008(3)
Mn—Mn/Fe	5.6(7)	3.05(2)	0.006(3)	6.2(6)	3.06(1)	0.008(3)	1.4(6)	2.06(1)	0.011(3)	1.5(7)	2.05(1)	0.008(3)
Mn—Mn/Fe	6.2(9)	3.49(3)	0.003(1)	3.9(7)	3.49(3)	0.003(1)	3.9(9)	3.01(3)	0.012(4)	3.6(9)	3.00(4)	0.011(4)
Mn—Mn/Fe	11(1)	5.28(4)	0.011(4)	13(1)	5.30(2)	0.010(4)	3.7(8)	3 .42(4)	0.014(5)	3.4(8)	3.40(5)	0.013(4)

For FM1 and FM2, the Mn—O distance is about 2.08 ± 0.01 Å, and the coordination numbers are 5.3 and 5.4 (Table 3), which is consistent with the theoretical value of octahedral Fe in the spinel structure of magnetite [25]. The Mn—Mn/Fe shell shows three distances (3.05 ± 0.01, 3.49 ± 0.01 and 5.29 ± 0.01 Å). They are also close to the Fe_{oct}—Fe_{oct}/Fe_{tet} distances of magnetite, indicating that the Mn cations have entered the spinel structure of magnetite and occupied the octahedral sites. In this case, two different substitution manners should exist, i.e., Mn cations replace the octahedral Fe in the bulk structure and they occupy the octahedral sites on the magnetite surface [49]. These two manners can be distinguished by the peak at 3.49 Å that is arisen from the Mn_{oct}—Fe_{tet} subshell. For FM1, the coordination number for this peak is 6.2, consistent with the theoretical one of Fe_{oct}—Fe_{tet} subshell in the bulk structure of magnetite. This suggests that Mn cations in FM1 mainly exist in the bulk of magnetite by substituting octahedral Fe (Fig. 4A). However, for FM2, the coordination number is just 3.9. Such obvious decrease in coordination number implies that partial Mn cations occupy the octahedral sites on magnetite surface (Fig. 4B).

For FM3 and FM4, the Mn—O and Mn—Mn/Fe distances and their coordination number are even lower than those of FM2 (Table 3), indicating the octahedral occupation on magnetite surface increases. To keep the charge equilibrium, some surface Mn cations with unoccupied atomic orbitals are bonded to the hydroxyls in the aqueous solution and even form a new phase feitknechtite, which is consistent with the observation from XRD. In the structure of feitknechtite, Mn cations are also octahedrally coordinated (Fig. 4C).

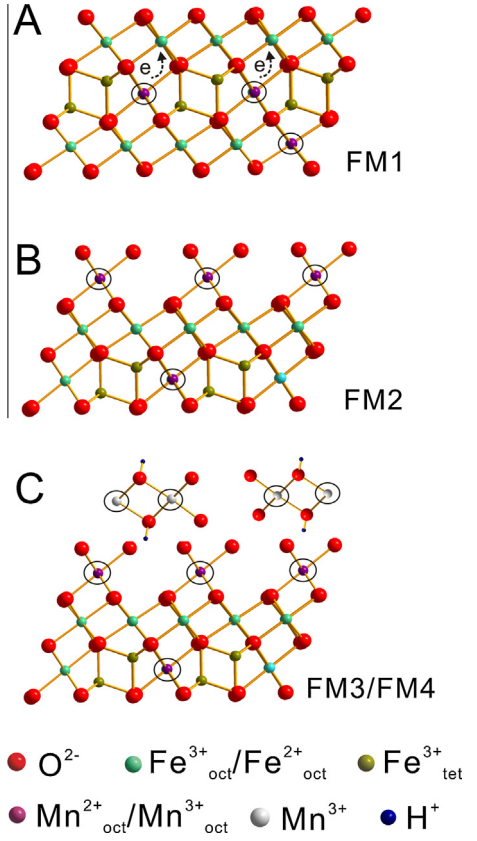

Fig. 4. Atom structure evolution of Mn substituted magnetite samples.

From the TG–DSC analysis under N_2, a mass loss can be seen on the TG curves from ca. 150 to 400 °C, which is assigned to the dehydroxylation [26,50]. The surface hydroxyl amount in the magnetite samples increases with the increase in Mn content (Table 1). This can be explained based on the variation of Mn coordination environment. From the EXAFS characterization, with the increase in Mn content, the proportion of Mn^{3+} increases and they prefer to occupy the octahedral sites on magnetite surface rather than the octahedral ones in the bulk structure. The surface Mn cations need to adsorb the hydroxyls in the aqueous solution to keep the charge equilibrium, which leads to the increase in surface hydroxyl amount.

3.3. Heterogeneous Fenton activity

The heterogeneous Fenton catalytic activity of Mn substituted magnetites was investigated through the AOII decolorization around neutral pH (Fig. 5A). Before adding H_2O_2, the decolorization of AOII only relied on its adsorption on magnetite surface. For all the systems, the removal efficiency of AOII by adsorption was quite low, below 3%. AOII is an anionic dye, whose pK_{a1} is 1.0 for the —SO_3H group and pK_{a2} is 11.4 for the naphthalene. On neutral pH, most of the dye molecules existed as anions. Since the point of zero charge (PZC) of magnetite is about 7.3 [51], the surface of magnetite samples was with weak negative charge and not favorable for the adsorption of AOII anions.

After the addition of H_2O_2, AOII decolorization was obviously accelerated. After 13 h of degradation, the AOII decolorization efficiency by FM0, FM1, FM2, FM3 and FM4 was 8%, 72%, 28%, 20% and 34%, respectively. The concentrations of dissolved Fe and Mn were below 0.5 mg L^{-1}, indicating that the whole decomposition process was dominated by heterogeneous process [52].

The degradation processes were analyzed in terms of kinetics (Fig. 5B). For FM1 with the highest degradation efficiency, the whole degradation process was well fitted with the pseudo-first-order kinetic equation (Eq. (1)). The apparent rate constant (K_{app}) is 1.68×10^{-3} min^{-1}. But for the other catalysts, their catalyzing processes were also fitted with the pseudo-first-order kinetic equation in the first 3 h, but then did not show obvious degradation. The apparent rate constant (K_{app}) in the initial 3 h for FM0, FM2, FM3 and FM4 was 6.0×10^{-6}, 1.2×10^{-3}, 5.5×10^{-4} and 1.25×10^{-3} min^{-1}, respectively. This indicates that the introduction of Mn greatly improved the heterogeneous Fenton catalytic activity of magnetite. Sample FM1 with the lowest Mn content in this study displayed the most efficient catalytic performance.

$$\ln(C_0/C_t) = K_{app}t \quad (1)$$

From previous studies [53,54], the degradation of organic pollutants in heterogeneous Fenton reaction followed the hydroxyl

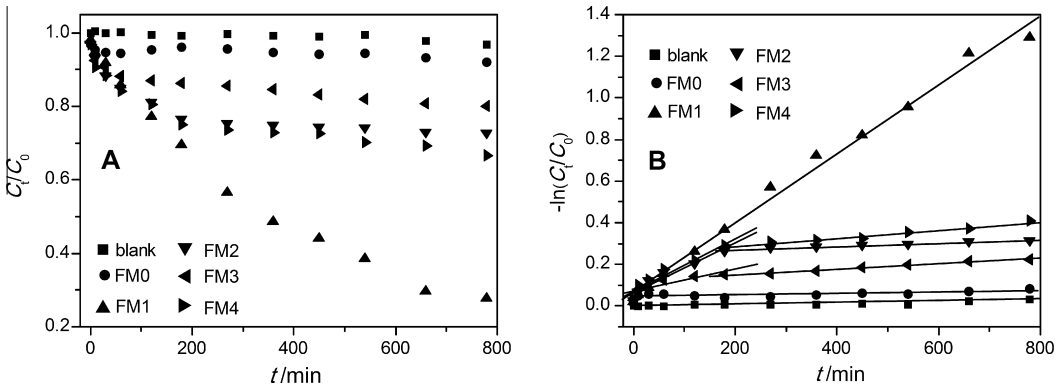

Fig. 5. Decolorization of Acid Orange II by Mn substituted magnetite samples in the presence of H_2O_2 (A) and its kinetics fitting by pseudo-first-order equation (B) (C_0 = 70 mg g^{-1}, 75 mmol L^{-1} of H_2O_2, 250 mg of catalyst, 250 mL, initial pH = 7.0, 25 °C).

radical-mediated mechanism. Hydroxyl radicals (·OH) were generated through the reaction between H_2O_2 and catalyst and then attacked the organic molecules. To further compare the catalytic activity of Mn substituted magnetites, the ·OH production in H_2O_2 decomposition was also traced (Fig. 6). The ·OH concentration approximately increased linearly as the reaction proceeded and was described by the zero-order equation (Eq. (2)). The apparent rate constant (k_{app}) for FM0, FM1, FM2, FM3 and FM4 was 0.0225, 0.728, 0.275, 0.198 and 0.154 μg L^{-1} min^{-1}, respectively. The ·OH production rate by Mn substituted magnetites was greatly higher than that by FM0. Sample FM1 showed the strongest catalytic activity, and other substituted samples did not show obvious difference in their catalytic performance, which is consistent to the observation from AOII degradation.

$$1 - C_t/C_0 = k_{app}t \quad (2)$$

In this study, Mn substitution significantly improved the heterogeneous Fenton activity of magnetite. But the improvement was not linearly related to the substitution extent. Sample FM1 with lower Mn content displayed the strongest activity, while for other samples, the activity did not vary obviously with the increase in Mn content. From previous studies [12,13], the strong Fenton activity of magnetite originates from the active species Fe^{2+} on magnetite surface and the fast electron transfer between octahedral Fe^{2+} and Fe^{3+}. The substitution of transition metals, e.g., Cr^{3+} [55] and V^{3+} [18], improved the Fenton activity of magnetite. It was ascribed to the acceleration of electron transfer by substituting cations to regenerate Fe^{2+}, and accordingly the intensification of H_2O_2 decomposition to produce ·OH (Fig. A.1). Such effects were greatly dependent on the occupancy of substituting metals. As the octahedral sites are almost exclusively exposed at the surface of the spinel structure, the catalytic activity relied on the octahedral Fe^{2+} rather than the tetrahedral ones [56].

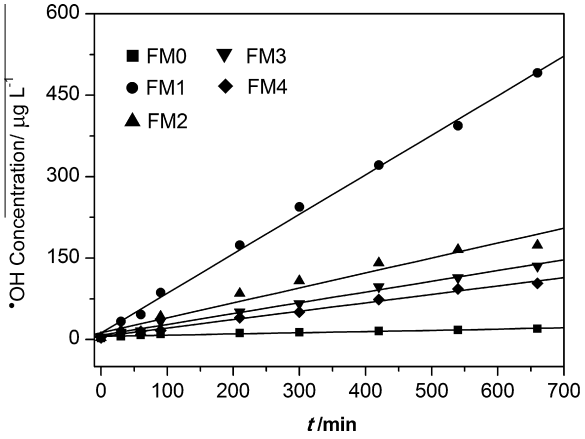

Fig. 6. The kinetics of ·OH radicals generation process catalyzed by Mn substituted magnetite samples in the presence of H_2O_2. (10 mmol L^{-1} of H_2O_2, 250 mg of catalyst, 250 mL, initial pH = 7.0, 25 °C).

From AOII degradation and ·OH generation test, the catalytic activity of magnetite varies significantly with Mn content, which should be related to the changes of Mn coordination environment (Fig. 4). For sample FM1, Mn cations mainly occupy octahedral sites in the bulk structure of magnetite (Fig. 4A). The octahedral Mn^{2+} and Mn^{3+} accelerate the electron transfer to regenerate the Fenton active species Fe^{2+}, which leads to the strong Fenton activity of FM1 (Fig. A.1) [13,23]. Moreover, the catalytic performance of magnetites with lower Mn substitution than FM1 (Table A.1) was tested in the AOII degradation. The XRD patterns of these samples just displayed the reflections of magnetite, indicating the pure spinel crystalline phase (Fig. A.2). The degradation processes were also fitted with the pseudo-first-order kinetic equation, and the degradation rate constants increased with the increase in Mn substitution (Fig. A.3). This suggests that, for the magnetite samples with lower Mn substitution than FM1, the Mn substitution gradually improved the Fenton catalytic activity of magnetite. From the EXAFS characterization, Mn cations in FM1 occupied the octahedral sites in the bulk structure of magnetite, and the Mn distribution on the octahedral sites of magnetite surface increased with an increase in Mn content. For the samples with Mn substitution lower than FM1, the Mn cations should mainly occupied the octahedral sites in the bulk structure. The increase in Mn cations in the bulk structure accelerated the electron transfer in the spinel structure during the degradation and accordingly improved the catalytic activity of the resultant magnetite.

But for the samples with higher Mn substitution than FM1, with the increase in Mn content, partial Mn cations replace Fe on the octahedral sites of magnetite surface. The decrease in superficial iron proportion on magnetite surface results in the decrease in active sites for Fenton reaction (Fig. 4B). For samples FM3 and FM4, some Mn cations exist as another phase feitknechtite, but were not incorporated into the magnetite structure, which retards the electron transfer between Fe and Mn cations (Fig. 4C). The above changes in coordination environment cause the weaker Fenton catalytic activity of FM2, FM3, FM4 than that of FM1. But the presence of Mn cations in the bulk structure in substituted magnetites still makes their Fenton reactivity higher than FM0.

3.4. Pb(II) adsorption

The effect of Mn substitution on the adsorption properties of magnetite for heavy metals was investigated in Pb(II) adsorption

experiments. The amount of adsorbed Pb(II) gradually increased with the increase in initial concentration and reached the maximum at the concentration of 300 mg L^{-1}(Fig. 7A).

The adsorption mechanism was discussed by Langmuir and Freundlich adsorption isothermal models. Langmuir model assumes that the adsorption takes place at specific homogeneous sites within the adsorbent and has been successfully applied in many monolayer adsorption processes. Its isotherm is represented by the following equation [57]:

$$C_e/q_e = C_e/q_m + 1/q_m b \quad (3)$$

where C_e describes the Pb(II) equilibrium concentration (mg L^{-1}); q_e represents the adsorbed amount of Pb(II) at equilibrium (mg g^{-1}); b is the Langmuir adsorption equilibrium constant (L mg^{-1}) and q_m denotes the maximum adsorption capacity corresponding to complete monolayer coverage (mg g^{-1}). Thus, a plot of C_e/q_e vs. C_e resulted in a straight line of slope ($1/q_m$) and an intercept of $1/bq_m$ (Fig. 7B). Table 4 shows the adsorption capacity q_m for all the magnetite samples. The q_m for FM0, FM1, FM2, FM3 and FM4 was 26.40, 26.92, 26.99, 30.68 and 36.27 mg g^{-1}, respectively. This indicates that the Mn substitution obviously improves the adsorption property of magnetite for Pb(II).

To determine whether the Pb(II) adsorption on magnetites was favorable or not for the Langmuir type adsorption process, the isotherm shape can be classified by a term "R_L", a dimensionless constant separation factor, which is defined in Eq. (4) [34]:

$$R_L = 1/(1 + bC_0) \quad (4)$$

Here, R_L is a dimensionless separation factor and C_0 is the initial concentration of Pb(II). The parameter R_L indicates the type of isotherm to be irreversible ($R_L = 0$), favorable ($0 < R_L < 1$), linear ($R_L = 1$) or unfavorable ($R_L > 1$). For all the adsorption systems, the calculated R_L values (Table 4) indicate the favorable adsorption of Pb(II) on all the magnetite samples.

The Freundlich isotherm is derived to model the multilayer adsorption. The linearized form of Freundlich model is formulated as Eq. (5) [57]:

$$\log q_e = \log k + 1/n \log C_e \quad (5)$$

where k is Freundlich constant roughly indicating adsorption capacity [(mmol g^{-1}) (mmol $L^{-1})^{-1/n}$] and n is an empirical parameter related to the adsorption intensity. The value of n varies with the heterogeneity of adsorbent, and for favorable adsorption process, the n value should lie in the range of 1–10. The value of k and n was calculated from the intercept and slope of linear plot of log q_e *vs* log C_e, respectively (Fig. 7C and Table 4). The k value indicating the adsorption capacity also increases with the Mn content, validating the positive effect of Mn substitution on the Pb(II) adsorption properties of magnetite.

The coefficient of determination R^2 is applied to determine the relationship between the experimental data and the isotherm in most studies. The R^2 values for linear form of Langmuir and Freundlich isotherms are in the range of 0.988–0.998 and 0.970–0.990, respectively. The Langmuir model yields a better linearity than the Freundlich model, indicating that the active sites for Pb(II) adsorption are homogeneous on magnetite surface.

The speciation of Pb(II) affects its charge properties and accordingly the adsorption by magnetite. Overall, the dominant form of Pb(II) at pH 2.0 is Pb^{2+} cation. With the increase in pH from 2.0 to 5.4, other species such as $Pb(OH)^+$ and $Pb_2(OH)^{3+}$ are formed [51]. At pH values above 5.4, precipitation of hydroxide ($Pb(OH)_2$) is observed (Fig. A.4). So at the adsorption pH of 4.5, Pb^{2+} was the dominant species. As the pH_{pzc} of magnetite samples were close to 7.0 (Table 1), all the magnetites were with positive charge at the adsorption pH. In this case, the Pb^{2+} adsorption should not rely on the electrostatic bonding. It was mainly through the complexation between the Pb^{2+} and deprotonated surface hydroxyl group [58]. Pb^{2+} acted as a Lewis while the functional surface hydroxyl group (≡M—OH) acted as Lewis basis in deprotonated form

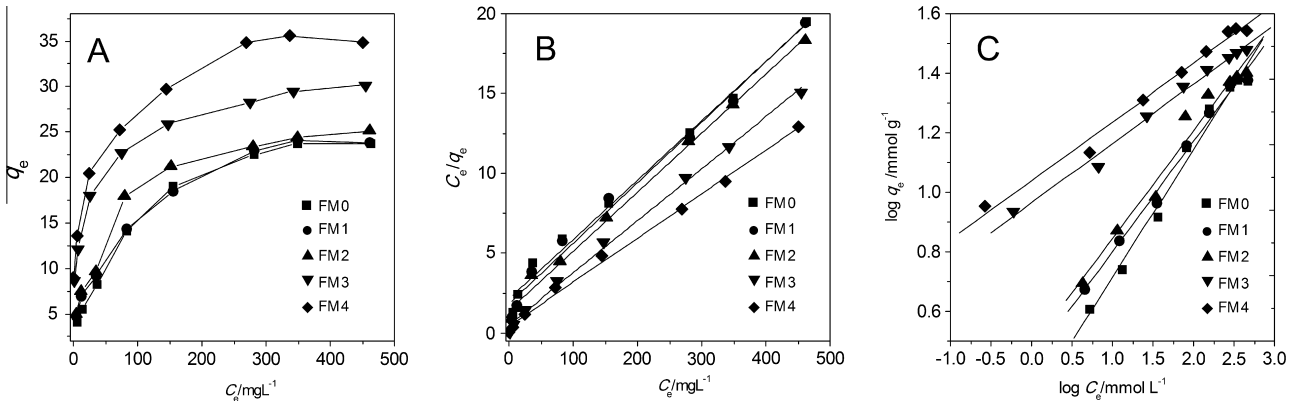

Fig. 7. Adsorption isotherms of Pb(II) on Mn substituted magnetite samples (A) and their Langmuir (B) and Freundlich (C) isotherms (50 mL Pb(II) solution, pH = 4.5, 25 °C, 50 mg of magnetite particles).

Table 4
Langmuir isotherm and Freudblich isotherm constants and adsorption equations of Pb(II) on Mn substituted magnetite samples.

Sample	Langmuir equation				Freudblich equation		
	q_m (mg g^{-1})	b (L mg^{-1})	R_L range	R^2	K (L g^{-1})	n	R^2
FM0	26.40	0.017	0.108–0.863	0.988	1.92	2.32	0.984
FM1	26.92	0.020	0.090–0.839	0.990	2.69	2.70	0.990
FM2	26.99	0.026	0.073–0.807	0.994	3.00	2.74	0.988
FM3	30.68	0.062	0.032–0.634	0.998	9.20	5.00	0.970
FM4	36.27	0.063	0.032–0.632	0.994	10.94	5.07	0.988

(≡M—O^-) to bind the Lewis acid Pb^{2+} cation [59]. The mono and binuclear inner-sphere complexes were formed (Eqs. (6) and (7)). Inner-sphere complexes were with coordinate-covalent bonding as the primary force and stable than the outer-sphere complexes in which electrostatic bonding was the main bonding force [59].

$$\equiv FeOH + Pb^{2+} \rightarrow FeOPb^{+} + H^{+} \quad (6)$$

$$\equiv (FeOH)_2 + Pb^{2+} \rightarrow (Fe-O)_2Pb + 2H^{+} \quad (7)$$

Obviously, as the Lewis basis, the surface hydroxyl group (≡M—OH) on magnetite was the key functional group in Pb^{2+} adsorption. From the XAFS and TG–DSC characterization, the surface hydroxyl amount for samples FM0, FM1, FM2, FM3 and FM4 was 0.64%, 1.42%, 2.16%, 2.27% and 2.31%, respectively. The Mn substitution increased the surface hydroxyl amount of magnetite, resulting in the improvement of Pb(II) adsorption. Moreover, the increase in specific surface area (Table 1) provided more contact field between magnetite surface and Pb(II), which should be another reason for the improvement of Pb(II) adsorption.

4. Conclusion

In the present study, a series of Mn substituted magnetites was characterized by XAFS and tested in catalyzing the heterogeneous Fenton degradation of acid orange II and Pb(II) adsorption. The Mn substituted magnetites show better catalytic activity than magnetite without substitution. The best catalytic efficiency is reached by the sample with the minimum Mn content, while the other Mn substituted magnetites show no obvious variations. The Pb(II) adsorption capacity of magnetite is gradually enhanced with the increase in Mn substitution.

The above different effects of Mn substitution on the catalytic activity and adsorption properties of magnetite are ascribed to the variations of Mn environment in magnetite. Mn cations initially occupy the octahedral sites in the bulk structure, accelerate the electron transfer and improve the catalytic activity of magnetite, which is in accordance with previous studies in Refs. [13,23]. But with an increase in Mn content, partial Mn cations occupy the octahedral sites on magnetite surface. This leads to a decrease in iron active species on magnetite surface and accordingly a decrease in catalytic activity.

Moreover, the Mn cations on magnetite surface adsorb hydroxyls to keep charge equilibrium, resulting in an increase in surface hydroxyl amount. The functional surface hydroxyl group acts as Lewis basis to bind the Lewis acid Pb^{2+} cations and form the inner-sphere complexes. So the increase in surface hydroxyl amount leads to the increase in Pb^{2+} adsorption. The inner-sphere complexes are more stable than the outer-sphere complexes. Due to the strong adsorption of Pb(II) on Mn substituted magnetite, this mineral should be an important attenuator of heavy metals. With the strong redox and adsorption properties, the effect of Mn substituted magnetite in the redox processes of heave metals (e.g., Cr and As) should be quite interesting and is under investigation.

The above results illustrate the remarkable effect of Mn substitution on the catalytic activity and adsorption properties of magnetite and would be benefit for the application of magnetite-group minerals in environment protection.

Acknowledgments

This is contribution No. IS-1858 from GIG CAS. We gratefully acknowledge Beijing Synchrotron Radiation Facility (BSRF) for providing us the beam time for the XAFS measurement. Financial supports were provided by National Natural Science Foundation of China (Grant Nos. 41172045, 41302026 and U1201233) and Shanghai Tongji Gao Tingyao Environmental Science & Technology Development Foundation (STGEF).

Appendix A. Supplementary material

Supplementary data associated with this article can be found, in the online version, at http://dx.doi.org/10.1016/j.jcis.2014.03.065.

References

[1] P.A. Xu, G.M. Zeng, D.L. Huang, C.L. Feng, S. Hu, M.H. Zhao, C. Lai, Z. Wei, C. Huang, G.X. Xie, Z.F. Liu, Sci. Total Environ. 424 (2012) 1.
[2] T. Zhou, X.H. Wu, Y.R. Zhang, J.F. Li, T.T. Lim, Appl. Catal. B-Environ. 136 (2013) 294.
[3] Y. Xu, L. Axe, N. Yee, J.A. Dyer, Environ. Sci. Technol. 40 (2006) 2213.
[4] H.T. Ren, S.Y. Jia, S.H. Wu, Y. Liu, C. Hua, X. Han, J. Hazard. Mater. 254 (2013) 89.
[5] A. Gajovic, A.M.T. Silva, R.A. Segundo, S. Sturm, B. Jancar, M. Ceh, Appl. Catal. B-Environ. 103 (2011) 351.
[6] X.S. Wang, F. Liu, H.J. Lu, P. Zhang, H.Y. Zhou, Desalination Water Treatment 36 (2011) 203.
[7] M. Usman, P. Faure, K. Hanna, M. Abdelmoula, C. Ruby, Fuel 96 (2012) 270.
[8] E.M. Moon, C.L. Peacock, Geochim. Cosmochim. Acta 104 (2013) 148.
[9] J.C. Barreiro, M.D. Capelato, L. Martin-Neto, H.C.B. Hansen, Water Res. 41 (2007) 55.
[10] S. Das, M.J. Hendry, J. Essilfie-Dughan, Appl. Geochem. 28 (2013) 185.
[11] J. Bandara, J.A. Mielczarski, J. Kiwi, Appl. Catal. B-Environ. 34 (2001) 307.
[12] A.L. Estrada, Y.Y. Li, A.M. Wang, J. Hazard. Mater. 227 (2012) 41.
[13] R.C.C. Costa, M.F.F. Lelis, L.C.A. Oliveira, J.D. Fabris, J.D. Ardisson, R.R.V.A. Rios, C.N. Silva, R.M. Lago, J. Hazard. Mater. 129 (2006) 171.
[14] L. Menini, M.C. Pereira, L.A. Parreira, J.D. Fabris, E.V. Gusevskaya, J. Catal. 254 (2008) 355.
[15] C.A. Gorski, J.T. Nurmi, P.G. Tratnyek, T.B. Hofstetter, M.M. Scherer, Environ. Sci. Technol. 44 (2010) 55.
[16] Y. Kuang, Q.P. Wang, Z.L. Chen, M. Megharaj, R. Naidu, J. Colloid Interf. Sci. 410 (2013) 67.
[17] E. Neyens, J. Baeyens, J. Hazard. Mater. 98 (2003) 33.
[18] X.L. Liang, S.Y. Zhu, Y.H. Zhong, J.X. Zhu, P. Yuan, H.P. He, J. Zhang, Appl. Catal. B-Environ. 97 (2010) 151.
[19] S.J. Yang, H.P. He, D.Q. Wu, D. Chen, X.L. Liang, Z.H. Qin, M.D. Fan, J.X. Zhu, P. Yuan, Appl. Catal. B-Environ. 89 (2009) 527.
[20] Y.H. Zhong, X.L. Liang, Y. Zhong, J.X. Zhu, S.Y. Zhu, P. Yuan, H.P. He, J. Zhang, Water Res. 46 (2012) 4633.
[21] X.L. Liang, Y.H. Zhong, H.P. He, P. Yuan, J.X. Zhu, S.Y. Zhu, Z. Jiang, Chem. Eng. J. 191 (2012) 177.
[22] C.G. Ramankutty, S. Sugunan, Appl. Catal. A-Gen. 218 (2001) 39.
[23] L.C.A. Oliveira, J.D. Fabris, R.R.V.A. Rios, W.N. Mussel, R.M. Lago, Appl. Catal. A-Gen. 259 (2004) 253.
[24] D. Carta, A. Corrias, A. Falqui, R. Brescia, E. Fantechi, F. Pineider, C. Sangregorio, J. Phys. Chem. C 117 (2013) 9496.
[25] M.Y. Zhang, G. Pan, D.Y. Zhao, G.Z. He, Environ. Pollut. 159 (2011) 3509.
[26] X.L. Liang, Y.H. Zhong, S.Y. Zhu, H.P. He, P. Yuan, J.X. Zhu, Z. Jiang, Solid State Sci. 15 (2013) 115.
[27] P. Yuan, M.D. Fan, D. Yang, H.P. He, D. Liu, A.H. Yuan, J.X. Zhu, T.H. Chen, J. Hazard. Mater. 166 (2009) 821.
[28] H.A. Wiatrowski, S. Das, R. Kukkadapu, E.S. Ilton, T. Barkay, N. Yee, Environ. Sci. Technol. 43 (2009) 5307.
[29] V.K. Mittal, S. Bera, S.V. Narasimhan, S. Velmurugan, Appl. Surf. Sci. 266 (2013) 272.
[30] A.C. Scheinost, L. Charlet, Geochim. Cosmochim. Acta 71 (2007) A886.
[31] D. Das, M.K. Sureshkumar, S. Koley, N. Mithal, C.G.S. Pillai, J. Radioanal. Nucl. Chem. 285 (2010) 447.
[32] H.B. Hu, Z.H. Wang, L. Pan, J. Alloy. Compd. 492 (2010) 656.
[33] L.S. Zhong, J.S. Hu, H.P. Liang, A.M. Cao, W.G. Song, L.J. Wan, Adv. Mater. 18 (2006) 2426.
[34] Y.M. Hao, M. Chen, Z.B. Hu, J. Hazard. Mater. 184 (2010) 392.
[35] T.B. Scott, G.C. Allen, P.J. Heard, M.G. Randell, Geochim. Cosmochim. Acta 69 (2005) 5639.
[36] M.L. Peterson, G.E. Brown, G.A. Parks, Colloid Surf. A 107 (1996) 77.
[37] X.L. Liang, Y.H. Zhong, W. Tan, J.X. Zhu, P. Yuan, H.P. He, Z. Jiang, J. Therm. Anal. Calorim. 111 (2013) 1317.
[38] W. Yu, T.L. Zhang, J.G. Zhang, X.J. Qiao, L. Yang, Y.H. Liu, Mater. Lett. 60 (2006) 2998.
[39] W.G. Hu, Y.L. Su, D.J. Sun, C.G. Zhang, Langmuir 17 (2001) 1885.
[40] H. Zegota, J. Chromatogr. A 863 (1999) 227.
[41] C. Tai, J.F. Peng, J.F. Liu, G.B. Jiang, H. Zou, Anal. Chim. Acta 527 (2004) 73.
[42] L.X. Chen, T. Liu, M.C. Thurnauer, R. Csencsits, T. Rajh, J. Phys. Chem. B 106 (2002) 8539.
[43] M. Wilke, F. Farges, P.E. Petit, G.E. Brown, F. Martin, Am. Mineral. 86 (2001) 714.
[44] A. Corrias, G. Ennas, G. Mountjoy, G. Paschina, Phys. Chem. Chem. Phys. 2 (2000) 1045.
[45] M. Magnuson, M. Andersson, J. Lu, L. Hultman, U. Jansson, J. Phys.-Condens. Matter 24 (2012).

[46] A. Manceau, M.A. Marcus, S. Grangeon, Am. Mineral. 97 (2012) 816.
[47] F. Farges, G.E. Brown, P.E. Petit, M. Munoz, Geochim. Cosmochim. Acta 65 (2001) 1665.
[48] M. Wilke, C. Schmidt, F. Farges, V. Malavergne, L. Gautron, A. Simionovici, M. Hahn, P.E. Petit, Chem. Geol. 229 (2006) 144.
[49] M.L. Peterson, G.E. Brown, G.A. Parks, C.L. Stein, Geochim. Cosmochim. Acta 61 (1997) 3399.
[50] R.M. Cornell, U. Schwertmann, The Iron Oxides: Structure, Properties, Reactions, Occurrences and Uses, Wiley.com, 2003.
[51] X.S. Wang, H.J. Lu, L. Zhu, F. Liu, J.J. Ren, Adsorpt. Sci. Technol. 28 (2010) 407.
[52] S.S. Chou, C.P. Huang, Y.H. Huang, Environ. Sci. Technol. 35 (2001) 1247.
[53] S.S. Lin, M.D. Gurol, Environ. Sci. Technol. 32 (1998) 1417.
[54] H. Zhou, Y.F. Shen, J.Y. Wang, X. Chen, C.L. O'Young, S.L. Suib, J. Catal. 176 (1998) 321.
[55] F. Magalhaes, M.C. Pereira, S.E.C. Botrel, J.D. Fabris, W.A. Macedo, R. Mendonca, R.M. Lago, L.C.A. Oliveira, Appl. Catal. A-Gen. 332 (2007) 115.
[56] C.G. Ramankutty, S. Sugunan, B. Thomas, J. Mol. Catal. A-Chem. 187 (2002) 105.
[57] M. Ozmen, K. Can, G. Arslan, A. Tor, Y. Cengeloglu, M. Ersoz, Desalination 254 (2010) 162.
[58] T.K. Sen, S.P. Mahajan, K.C. Khilar, Colloid Surf. A 211 (2002) 91.
[59] H.B. Bradl, J. Colloid Interf. Sci. 277 (2004) 1.